NAVAL POSTGRADUATE SCHOOL

MONTEREY, CALIFORNIA

THESIS

EFFECTS OF FEMTOSECOND LASER SURFACE PROCESSING ON HYDRODYNAMIC DRAG OVER A FUNCTIONALIZED SURFACE

by

Dillan A. Masellas

June 2018

Thesis Advisor: Young W. Kwon
Second Reader: Jarema M. Didoszak

THIS PAGE INTENTIONALLY LEFT BLANK

REPORT DOCUMENTATION PAGE			*Form Approved OMB No. 0704-0188*

1. AGENCY USE ONLY *(Leave blank)*	**2. REPORT DATE** June 2018	**3. REPORT TYPE AND DATES COVERED** Master's thesis

4. TITLE AND SUBTITLE EFFECTS OF FEMTOSECOND LASER SURFACE PROCESSING ON HYDRODYNAMIC DRAG OVER A FUNCTIONALIZED SURFACE	**5. FUNDING NUMBERS**
6. AUTHOR(S) Dillan A. Masellas	
7. PERFORMING ORGANIZATION NAME(S) AND ADDRESS(ES) Naval Postgraduate School Monterey, CA 93943-5000	**8. PERFORMING ORGANIZATION REPORT NUMBER**
9. SPONSORING / MONITORING AGENCY NAME(S) AND ADDRESS(ES) N/A	**10. SPONSORING / MONITORING AGENCY REPORT NUMBER**

11. SUPPLEMENTARY NOTES The views expressed in this thesis are those of the author and do not reflect the official policy or position of the Department of Defense or the U.S. Government.

12a. DISTRIBUTION / AVAILABILITY STATEMENT Approved for public release. Distribution is unlimited.	**12b. DISTRIBUTION CODE** A

13. ABSTRACT (maximum 200 words)

Femtosecond laser surface processing (FLSP) is capable of creating several structures on a variety of metallic surfaces that change its hydrodynamic properties. This research focused on the skin friction effects of superhydrophobic and superhydrophilic surface treatments by FLSP. Each type of hydrodynamic surface treatment was studied in the below surface growth (BSG) and the above surface growth (ASG) microstructure form and compared to the performance of a control plate of identical dimensions without a treated surface. The stability of the Cassie state in a fully submerged environment was assessed using an optical microscope. The BSG superhydrophobic surface treatment was submerged in seawater to examine its resistance to biological growth. The BSG superhydrophobic surface treatment's resistance to biofouling is limited and microstructures appear to provide for adhesion of organisms to the surface.

Submerged testing in a rectangular water channel used variable flow rates to achieve Reynolds numbers ranging from 20,000 to 70,000 based on the size of the test sample. Results of these tests showed that the superhydrophilic surface treatments have the same hydrodynamic drag properties as a smooth surface. The superhydrophobic-treated surfaces are ineffective at this range of flow rate due in part to the poor integrity of the trapped Cassie state under static- and flow-induced pressures.

14. SUBJECT TERMS femtosecond laser surface processing, FLSP, superhydrophobic, superhydrophilic	**15. NUMBER OF PAGES** 55
	16. PRICE CODE

17. SECURITY CLASSIFICATION OF REPORT	**18. SECURITY CLASSIFICATION OF THIS PAGE**	**19. SECURITY CLASSIFICATION OF ABSTRACT**	**20. LIMITATION OF ABSTRACT**
Unclassified	Unclassified	Unclassified	UU

NSN 7540-01-280-5500 Standard Form 298 (Rev. 2-89) Prescribed by ANSI Std. 239-18

THIS PAGE INTENTIONALLY LEFT BLANK

Approved for public release. Distribution is unlimited.

EFFECTS OF FEMTOSECOND LASER SURFACE PROCESSING ON HYDRODYNAMIC DRAG OVER A FUNCTIONALIZED SURFACE

Dillan A. Masellas
Lieutenant Commander, United States Navy
BS, Maine Maritime Academy, 2007

Submitted in partial fulfillment of the
requirements for the degree of

MASTER OF SCIENCE IN MECHANICAL ENGINEERING

from the

NAVAL POSTGRADUATE SCHOOL
June 2018

Approved by: Young W. Kwon
Advisor

Jarema M. Didoszak
Second Reader

Garth V. Hobson
Chair, Department of Mechanical and Aerospace Engineering

THIS PAGE INTENTIONALLY LEFT BLANK

ABSTRACT

Femtosecond laser surface processing (FLSP) is capable of creating several structures on a variety of metallic surfaces that change its hydrodynamic properties. This research focused on the skin friction effects of superhydrophobic and superhydrophilic surface treatments by FLSP. Each type of hydrodynamic surface treatment was studied in the below surface growth (BSG) and the above surface growth (ASG) microstructure form and compared to the performance of a control plate of identical dimensions without a treated surface. The stability of the Cassie state in a fully submerged environment was assessed using an optical microscope. The BSG superhydrophobic surface treatment was submerged in seawater to examine its resistance to biological growth. The BSG superhydrophobic surface treatment's resistance to biofouling is limited and microstructures appear to provide for adhesion of organisms to the surface.

Submerged testing in a rectangular water channel used variable flow rates to achieve Reynolds numbers ranging from 20,000 to 70,000 based on the size of the test sample. Results of these tests showed that the superhydrophilic surface treatments have the same hydrodynamic drag properties as a smooth surface. The superhydrophobic-treated surfaces are ineffective at this range of flow rate due in part to the poor integrity of the trapped Cassie state under static- and flow-induced pressures.

THIS PAGE INTENTIONALLY LEFT BLANK

TABLE OF CONTENTS

THIS PAGE INTENTIONALLY LEFT BLANK

LIST OF FIGURES

LIST OF TABLES

THIS PAGE INTENTIONALLY LEFT BLANK

LIST OF ACRONYMS AND ABBREVIATIONS

ASG	Above Surface Growth
BSG	Below Surface Growth
CA	Contact Angle
CVD	Chemical Vapor Disposition
FLSP	Femtosecond Laser Surface Processing
PVA	Polyvinyl Alcohol
SA	Sliding Angle

THIS PAGE INTENTIONALLY LEFT BLANK

ACKNOWLEDGMENTS

My thanks go out to Dr. Kwon and Jarema Didoszak for providing for this research with such enthusiasm. I also need to thank my wife for her mission-focused understanding during the many weekends of research, and our daughter for being proud of me.

THIS PAGE INTENTIONALLY LEFT BLANK

I. INTRODUCTION

A. BACKGROUND

In the face of a rising global demand for energy and declining traditional energy resources, the scientific community is working harder than ever to reduce waste and improve efficiency through technological innovation. Fluid systems are ubiquitous in our daily lives and an area in which simply reducing friction could significantly reduce operating costs and our impact on the environment. For the U.S. Navy, the Office of Naval Research is researching new ways to reduce friction in our fluid systems to keep our nation's defenders ready for the future.

When a viscous fluid travels along a solid boundary, such as within a pipe, we assume that there is no relative motion between the two materials where they come in contact at the molecular level [1]. This, the no-slip boundary condition, is a universally recognized principle in fluid dynamics that drives the design of technology today. The no-slip boundary condition results in drag and pressure loss from friction as a fluid travels along the solid boundary. This assumption in the Navier-Stokes equations and extensive experimentation have proven the no-slip condition to be an adequate approximation for fluid modeling and system design [2].

The concept of a slip condition, or relative motion at the fluid boundary, presented by Navier in 1823 [3], concludes that relative motion between a fluid and a solid at the point of contact would be proportional to the slip length of the surface, and fluid shear rate. In the presence of a slip condition, a fluid system would have lower skin friction, and therefore, consume fewer resources and produce less waste. Figure 1 is an illustration of how slip can influence fluid motion along a boundary where β is the slip length.

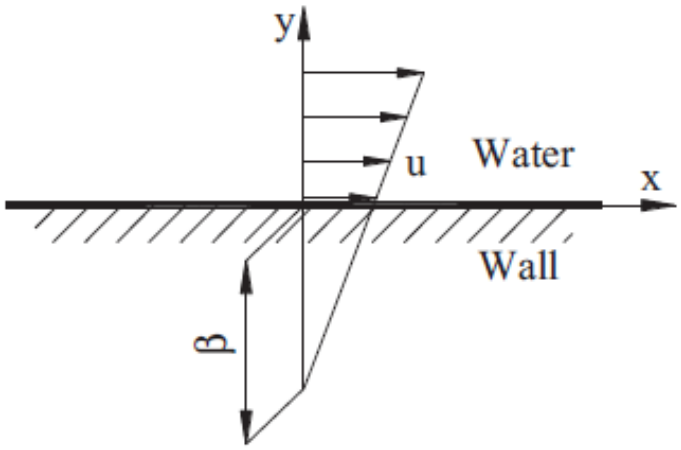

Figure 1. Wall velocity with slip length. Source: [2].

A hydrophobic surface has features that allows slip between the fluid and solid boundary [4], which reduces the effect of skin friction along the boundary. Effects of hydrophobicity appear in nature in such forms as lotus leaves and rose petals. The term "lotus effect" refers to the self-cleaning properties of lotus leaves manifested through a droplet's tendency to roll along its surface and collect debris [5]. The opposite effect, known as hydrophilicity, is also present on leaves in nature that have a wicking effect when wetted. In the case of the hydrophilic surface, a fluid will have a tendency to adhere to the surface and increase friction [6]. In the naturally occurring examples of hydrophobicity and hydrophilicity, surface energy changes through coatings and micrometer- and nanometer-scale surface features are the mechanisms of wetting resistance or wettability [5], [7]. Wenzel's original model [8] for determining the contribution of roughness to hydrophobicity considers changes in net energy as a droplet spreads over a surface. A rougher surface has a lower net energy by way of surface area, which serves to increase the surface's hydrophobic or hydrophilic behavior. Scientific advances in nanotechnology and material science have recently allowed for the manipulation of artificial surfaces such that they exhibit hydrophobic and hydrophilic properties through micro/nanoscale changes in surface roughness [9]. Burton and Bhushan showed that for a given hydrophobic or hydrophilic surface, increasing surface roughness serves to enhance the preexisting effects

[10]. Consequently, micro and nanoscale surface structures that can modify the slip condition is an enthusiastically studied field around the world today.

B. HYDROPHOBIC AND HYDROPHILIC SURFACES

A material's hydrophobicity or hydrophilicity is qualitatively determined by measuring its contact angle (CA). Superhydrophobicity includes measurement of a surface's contact hysteresis, or sliding angle (SA) [11]. Each parameter is a measurement related to the behavior of a drop of water on a flat surface. The CA is determined by measuring the angle between the curve of the droplet and the solid boundary where the two come into contact. The SA is the measured by rotating the level surface to the angle where the droplet begins to move under the force of gravity and measuring the distortion between the leading and trailing edges of the droplet. Figure 2 shows the referencing method for determining CA. Figure 3 diagrams the tilting plate method for determining SA.

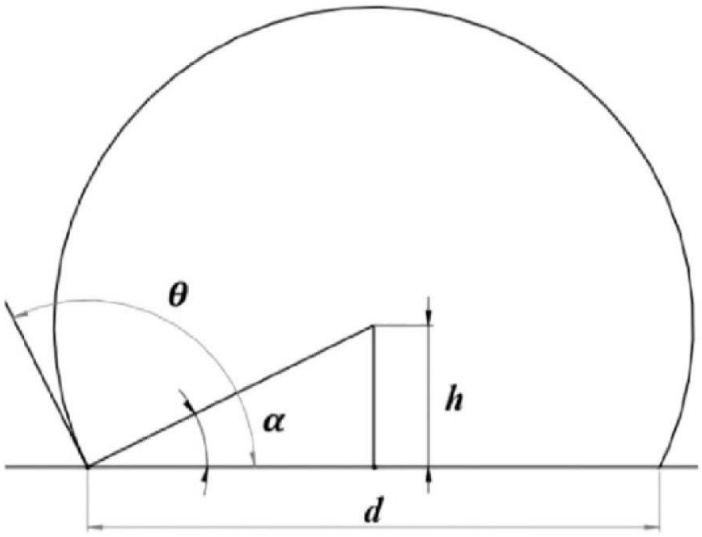

Figure 2. Contact angle reference. Adapted from [12].

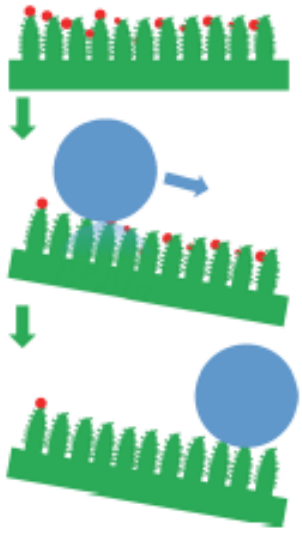

Figure 3. Sliding angle reference. Adapted from [11].

A surface is determined to be hydrophobic if it exhibits a CA greater than 90 degrees whereas hydrophilic surfaces exhibit a CA less than 90 degrees [8]. Superhydrophobic surfaces feature a CA between 150 and 180 degrees and SA less than 10 degrees, which are the conditions of the Cassie state [13]. In the Cassie state, shown in Figure 3, a volume of air between fluid and solid serves to provide a slip length provided by the much higher shear rate of air and limited by the fluid's interaction with the peaks of the solid formations. Features on the surface such as size, spacing, and secondary structures, and chemistry can significantly alter the stability of the Cassie state [11], [12]. If the air pocket collapses, the droplet can fall into the gap between the peaks, which yields the Wenzel state or wetting of the surface [14] such as depicted in Figure 4.

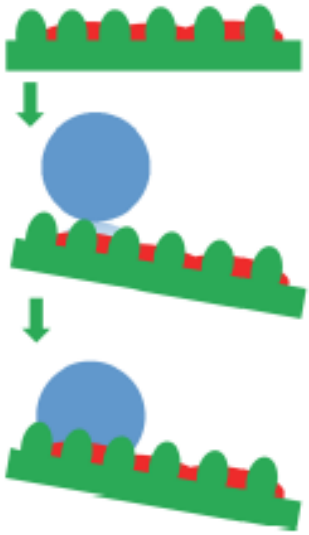

Figure 4. Transition from Cassie to Wenzel state. Adapted from [11].

There are many possible applications for both superhydrophobic and superhydrophilic surface properties both derived from and unrelated to surface friction. For example, Ou et al. [15] showed that superhydrophobic surfaces improved laminar mixing in microfluidic devices by an order of magnitude with shear-free surface channels. Kim et al. [15] used numerical simulations to show improved flow stability in high-Reynolds number flows. The presence of a superhydrophilic surface would improve boiling heat transfer [16] and critical heat flux [17] in nuclear reactors by keeping a hot surface wetted with coolant. Superhydrophilic properties are also beneficial in oil/water separation [18] and similar environmental cleanup applications.

C. MICRO/NANOSCALE SURFACE PROCESSING

As vast as the range of applications for hydrophobic and hydrophilic properties is the range of materials and methods of achieving such states. The total surface area of the solid, the fluid environment and viscosity, and durability of the surface are limiting application factors driving the development of new micro/nanoscale surface processing methods [11]–[14].

Feng et al. [19] used a membrane of anodic aluminum oxide to extrude amphiphilic polyvinyl alcohol (PVA) nanotubes from film on a glass slide. The amphiphilic PVA is not naturally hydrophobic, so introducing roughness would not normally create a hydrophobic condition. However, the extrusion process served to arrange the polymer's hydrogen bonds in such a way as to create a hydrophobic condition at the surface of the fibers. The PVA film was hydrophilic with a CA of only 71 degrees. Following the extrusion process, the PVA fibers shown in Figure 5 tested with a CA of about 171 degrees. This process showed that it is possible to take a normally hydrophilic flat surface and create a superhydrophobic surface with nanoscale roughness. Extruded polymers raise questions about durability and effective surface area, so the application of this method is limited.

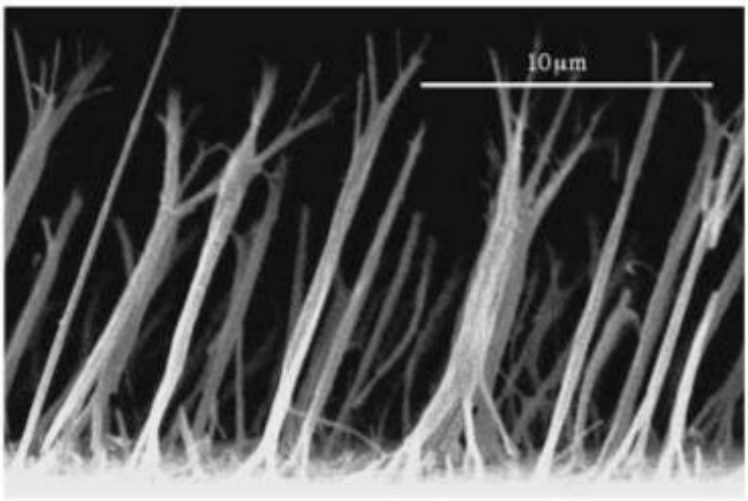

Figure 5. SEM image of nanoscale PVA fibers. Source: [19].

Lithography is a way of combining microstructural and chemical approaches to achieve a superhydrophobic or superhydrophilic surface. Etching generates a patterned surface roughness on a substrate. The etched surface, coated with a hydrophobic material as in Figure 6, creates a superhydrophobic condition that is capable of reducing microfluid system resistance by over 99% [20]. The etched surfaces may not have hydrophobic properties alone, but the nature of the surface roughness lends itself to coating with materials such as Teflon. The hydrophobic property of the Teflon is enhanced by the

roughness of the substrate. Tadanaga et al. [21] coated a substrate of aluminum oxide, whose nanoscale roughness was created with boiling water, with fluoroalkylsilane to create a superhydrophobic surface. Using a more advanced method; Youngblood and McCarthy [22] created an ultrahydrophobic polypropylene surface by combining etching processes with radio frequency plasma depolymerization of polytetrafluoride. Lithography methods utilizing photo or laser etching are more effective in microscale applications because of the prohibitive time and cost of the processes [21].

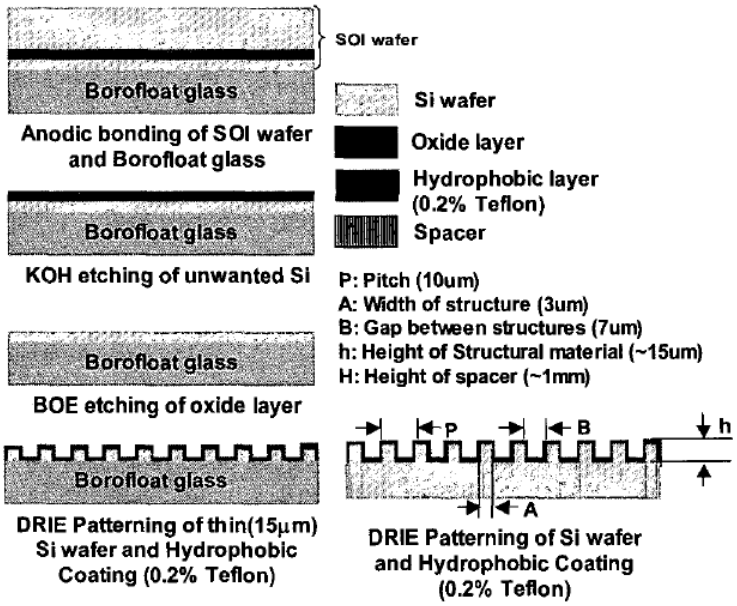

Figure 6. Graphical depiction of lithography method employed by Kim et al. Adapted from [20].

In most cases of coatings, durability and stability are the primary drawbacks. Chemical Vapor Disposition (CVD) attempts to use a durable film and strong chemical bonding with the substrate to create a stable superhydrophobic surface. Liu et al. [23] achieved a stable superhydrophobic surface with a zinc oxide film and a gold catalyst with nanoscale features presented in Figure 7. Sapphire substrates were coated with gold, then heated in a furnace with zinc oxide and carbon powders as the deposition material. The structures formed by the zinc oxide on the gold had nanoscale structures desirable for maintaining the Cassie state, with air trapped under the water droplet. This surface was

also reversible to a hydrophilic state under UV light, as well as recoverable to a hydrophobic state when heated or left in the dark. This chemical disposition method used high cost materials to produce a zinc oxide surface structure that raises concern for size and durability and size as much as the methods already discussed.

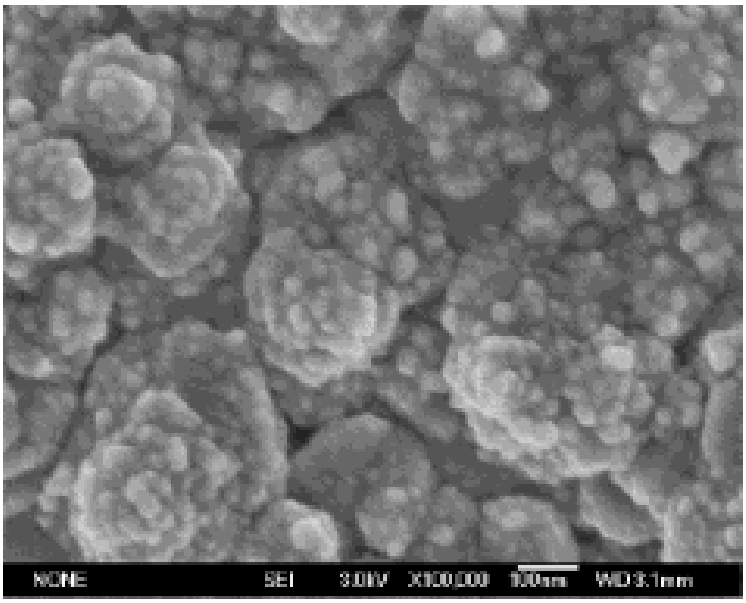

Figure 7. Superhydrophobic nanostructures from chemical disposition. Adapted from [23].

Nanotubes have a vast array of applications, so it is no surprise indeed that they are capable of creating superhydrophobic surface condition. Donghyun Kim et al. [24] created hierarchal structures similar to that on a lotus leaf by dipping anodized porous aluminum in a solution with Teflon. The Teflon adhered to the surface of the aluminum, filling the porous aluminum structures. Once the aluminum was chemically removed, only nano-wire Teflon structures remained that, like those formed by lithography, displayed substantial superhydrophobic properties. Recently, Sethi et al. [25] created a more durable nanotube coating that they grew on a porous 304 Stainless Steel plate. The steel provided structural and conductive capacity while the elastomer-reinforced nanotube structures withstood a pencil scratch and adhesion test. However, the high temperature conditions and inert

environment required for growth of these carbon nanotubes limits large-scale industrial application.

D. FEMTOSECOND LASER SURFACE PROCESSING

Laser irradiation, like the methods already discussed, has the ability to create micro- and nano-scale structures on virtually any surface that is subject to ablation. Femtosecond Laser Surface Processing (FLSP) uses high frequency pulse width modulation to created micro- and nano-scale structures on smooth solid surfaces. By varying the pulse duration and frequency of the laser, surface texturing can be modified to meet the requirements of the material or application.

Early applications of FLSP used non-reflective surfaces on silicone [26] and polymer [27] surfaces. The softer materials' initial surface energy means that they can become superhydrophobic by adding roughness, much in the same way that lithographic methods achieved such a state. Metallic structures created by laser ablation have inherent durability and reliability, but lack the surface energy to be superhydrophobic without an alteration of the surface energy. Kietzig et al. [28] found that superhydrophobicity on initially hydrophilic metallic surfaces is achieved with the addition of carbon to provide a chemical surface alteration not unlike the polymer extrusions created by Feng et al. [number?]. Carbon built up over a period of months on the surface of stainless steel microstructures with exposure to carbon dioxide that reacted with ferrite formed during ablation [28]. Kietzig et al. [28] also noted that higher fluence (energy per unit area) created more roughness and increased the time for carbon absorption to produce a CA greater than 150 degrees. With the idea of varying fluence to change nanoscale surface features, Zuhlke et al. [29] developed the Above Surface Growth (ASG) and Below Surface Growth (BSG) nano-scale pyramids with secondary features on nickel. BSG mounds were formed by ablated valley formation. Higher fluence caused growth by uneven heating and redeposition of ablated material to create ASG formations [29]. These surfaces, when treated with carbon to obtain superhydrophobic properties, maintain their properties when completely submerged in water for about 40 days [30]. The size of the crystalline structures of metals like stainless steel and titanium correlates with the pyramid dimensions,

indicating that grain boundaries may the origin of their growth [31]. However, Peng et al. [32] have used FLSP to produce BSG and ASG structures on large scale amorphous and polycrystalline nickel alloy plates that do not correlate to grain boundaries.

The use of FLSP on stainless steel and titanium has resulted in a simple and repeatable means of creating large superhydrophobic surfaces. These structural materials have potential for optimized use in critical industrial applications where friction losses or heat transfer can significantly improve performance and reduce waste.

E. OBJECTIVE

The objective of this research is to analyze the performance of FLSP hydrophobic and hydrophilic surfaces on functionalized 304 stainless steel plates for industrial applicability. Submerged testing is performed in a water tunnel to evaluate air film retention and skin drag reduction on the superhydrophobic surfaces over a range of Reynold's numbers for each BSG and ASG surface geometries. The BSG and ASG hydrophilic samples will be tested in a similar manner to determine differences in skin drag performance between the two types pyramid structures. The BSG hydrophobic surface will be tested for its resiliency against biological growth and fouling.

II. EXPERIMENT DESIGN

A. FLOW CHANNEL SETUP

The water channel and test stand used in this experiment was designed and constructed by James Ley [33] for the purpose of analyzing functionalized hydrophobic surfaces in a submerged flow field over a range of Reynold's numbers. The composite system configuration is shown in Figure 8.

Figure 8. Water channel and test stand

The test stand consists of a variable speed pump on vibration dampening mounts that takes suction from a 189.27 L (50 gal.) water drum. The pump is capable of sending 227.12 – 832.79 L/min (60 – 220 gpm) to the downstream water drum. The flow into the downstream drum causes a pressure differential between the drums that induces the flow through the test section at a stable rate that is proportional to pump speed.

The flow channel is constructed of 25.4 mm (1.0 in) acrylic and is mounted at about half-height of each drum so adequate net positive suction head can be provided to the pump while ensuring a broad range of flow rates are available to the water channel. Flow velocity

is monitored downstream of redundant flow conditioners using an ultrasonic flow meter with a digital readout that is mounted on the side of the water channel. The removable specimen fixture is located downstream of the flow meter and held in place with a removable acrylic cover. The specimen stand is T-6061 aluminum and houses the parallel pendulum harnesses and sensor stanchions as arranged in Figure 9.

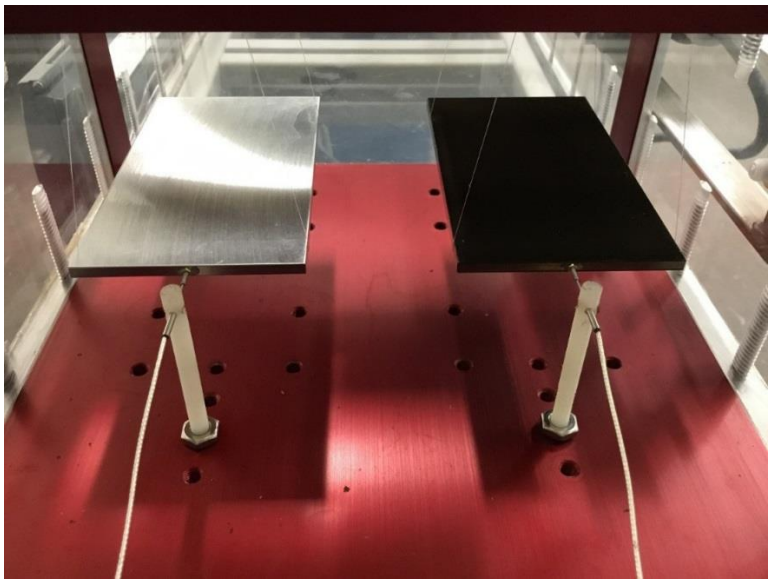

Figure 9. Parallel specimens and sensing system mounted in specimen stand

The specimen plates are 3 mm (0.12 in) thick by 57.15 mm (2.25 in) wide by 101.6 mm (4.0 in) long. Plates were prepared with a 00–90 UNC brass nut attached with epoxy to the trailing edge to accept the threaded sensor core and symmetrically mounted in the parallel pendulum arrangement with single strand nylon thread for minimal flow interference.

The sensing system measures average longitudinal displacement of a test specimen over a large range of flow conditions. The displacements were measured using Lord MicroStrain Demod-DVRT®-2 Signal Conditioners [34] calibrated with Lord Microstrain Subminiature DVRT®. The sensors measured displacement up to 3 mm (0.12 in) of stroke over a 5.0V linear output with resolution <1.0 μm (4.0e-5 in). Analog voltage from the signal conditioners was converted through a National Instruments 10V A-D converter at

500 kS/s. Data acquisition software recorded 1 kS/s with a 28.7 Hz low-pass filter for fluid flow and test stand oscillations.

B. DISPLACEMENT TESTING

The plates tested for skin friction effects in the flow channel were the BSG superhydrophobic, ASG superhydrophobic, BSG superhydrophilic, and ASG Superhydrophilic types. Two control plates were prepared and tested.

Two plates were mounted in each of the two double pendulum swings for each test. Each displacement sensor core was threaded into the nut on the rear of the associated test plate and carefully aligned with the sensor sleeve. Before the system was filled, each plate and sensor pair was adjusted to ensure that there was a positive observable deflection in voltage output from the rested position and that there were no friction or sticking points inside the sensor across the stroke of the core while it traveled with the plate. A close-up of a plate pair prepared and aligned for testing is provided in Figure 10.

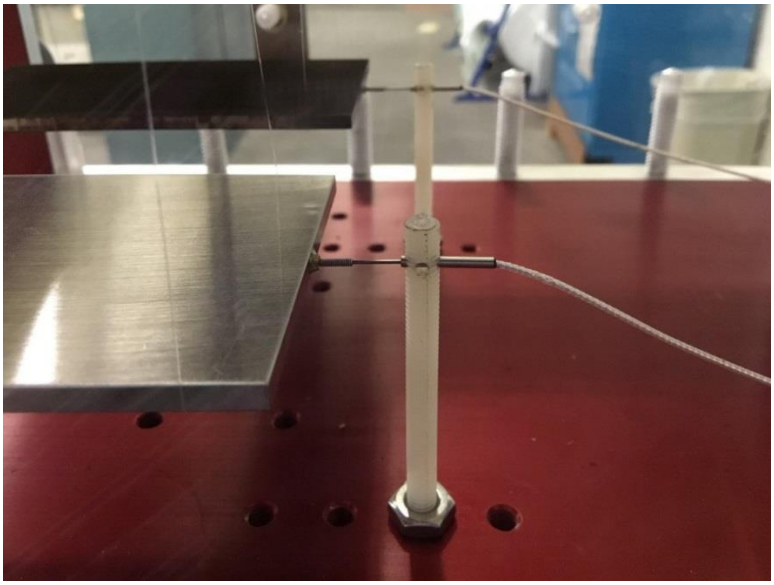

Figure 10. Control plate prepared with displacement sensor

Once the plate motion was both smooth and observable, the system was closed and filled with distilled water. The water level in each drum was raised to approximately 360

mm (14.17 in) above the test plates to provide adequate net positive suction head to the pump at high speeds.

While observing voltage output, the pump was started at its lowest speed and after flow stabilized and plates had been observed to move freely, baseline voltage output was recorded for 60 seconds. Once the baseline was recorded, the pump speed was raised and the process repeated for each of 10 higher speed settings to obtain a complete set of data. Free motion was again verified as the pump speed was gradually reduced to idle.

Data sets for each of the five plate types were recorded on both sensors to identify possible sensor bias and eliminate subtle differences in configurations between each pendulum and sensor set. The voltage output was correlated to the sensor calibration data to determine the force required to cause the pendulum motion and curves were plotted using Reynolds number as the independent variable. The difference in drag force from skin friction was assessed as the difference in total force from the control plate.

C. OBSERVING CASSIE STATE STABILITY

The stability of the Cassie state for the BSG Superhydrophobic and ASG superhydrophobic test plates was determined visually using a Dino-Lite Edge® AM73915MZTL digital USB microscope [35]. Tests were conducted in a fully submerged environment using distilled water in the flow channel.

The presence and duration of the Cassie state on the surface of each plate was observed using static pressure by incrementally raising the level of the water in the flow channel. Once the system was full, the pump was operated for twenty minutes at 1100 rpm while both plates were observed for the presence of an air layer on the surface. Magnified images of each plate surface were captured at transition points throughout the tests. Figure 11 shows the arrangement of the microscope and the depth of the water used in the static portions of the test.

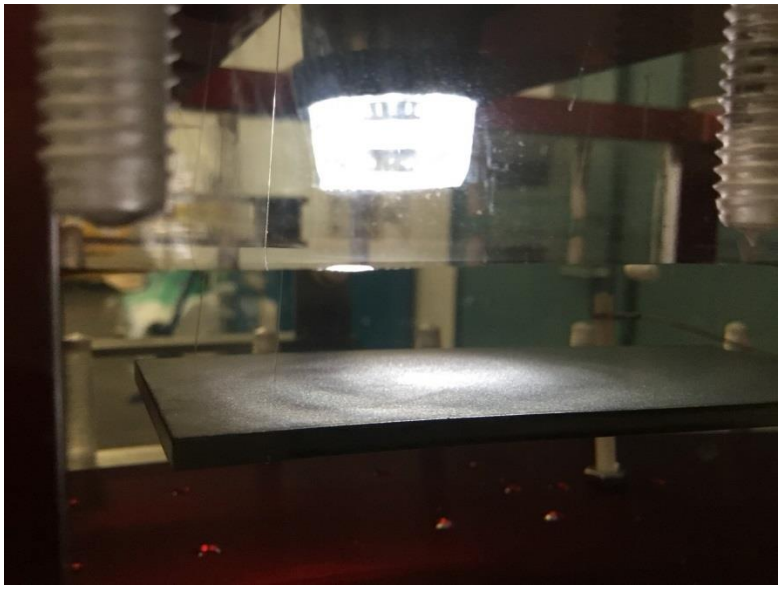

Figure 11. Cassie state stability observation arrangement

D. BIOFOULING TEST

The BSG superhydrophobic test plate was assessed for biological growth resistance by submerging it in seawater in a local active pier in Monterey Bay for 24 days. The test used a BSG superhydrophobic plate sample housed inside an open-ended polymer tube that was suspended by a frame below a floating dock, as shown in Figure 12. The timeline for expected biological growth was derived from an antifouling technology paper published by Yebra et al. [36]. Figure 13 shows the expected growth timeline for organisms on a similar metallic surface. Representative photos were taken to show the relative difference in the rate of adhesion of biological organisms between the control plate and the BSG superhydrophobic plate over the duration of the test. Weights were not recorded, as testing conditions precluded the drying and cleaning normally associated with corrosion tests.

Figure 12. Biofouling test environment

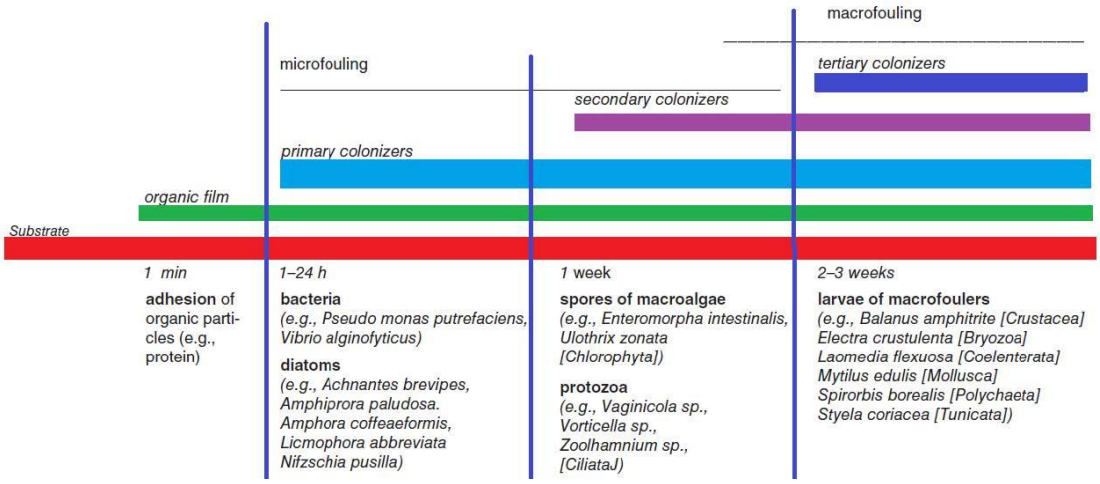

Figure 13. Biofouling timeline. Source: [36].

III. RESULTS

A. DISPLACEMENT TESTS

Table 1 relates the pump speeds in the tests to Reynold's Number used for displacement analysis.

Table 1. Reynolds number as related to pump speed

Pump Speed (rpm)	Flow Velocity m/s (ft/s)	Re#
1100	0.2353 (0.7720)	23790
1250	0.2506 (0.8222)	25340
1500	0.2735 (0.8974)	27660
1750	0.3200 (1.0498)	32350
2000	0.3728 (1.2232)	37700
2250	0.4309 (1.4137)	43570
2500	0.4844 (1.5892)	48980
2750	0.5348 (1.7546)	54080
3000	0.5898 (1.9351)	59640
3250	0.6448 (2.1156)	65200
3450	0.6723 (2.2058)	67980

Computed in terms of test plate dimensions.

Each FLSP treated plate and control plate was tested several times to obtain data sufficient to average out random errors due to flow instability and sensor noise. The data was consistent for each of the plate tests within the accuracy of the system with minimal outliers. Voltage output from each sensor was correlated to displacement in millimeters using a polynomial fit function provided by the manufacturer with the calibration data in Appendix A. The lowest pump speed, 1100 rpm, was used as the baseline for each of the tests to ensure a calibrated zero position was referenced for each iteration. Displacement data from the test sets are shown plotted against the control results in Figures 14–17. Since the plates are all of nearly identical mass and dimension, these displacements are proportional to total drag force.

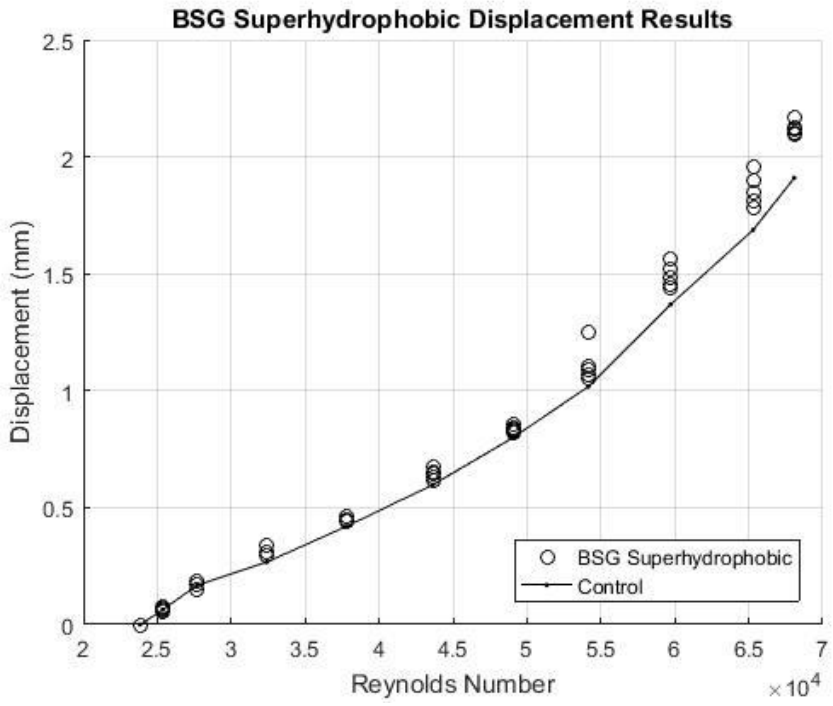

Figure 14. Displacement results from BSG superhydrophobic tests

The BSG superhydrophobic results are counterintuitive given the expectation of reduced skin friction. The near linear increase in displacement difference from the control as Reynolds number increases is indicative of a rough surface rather. The consistency of these results led to the Cassie state stability tests that served to explain the performance of the BSG superhydrophobic treatment when fully submerged.

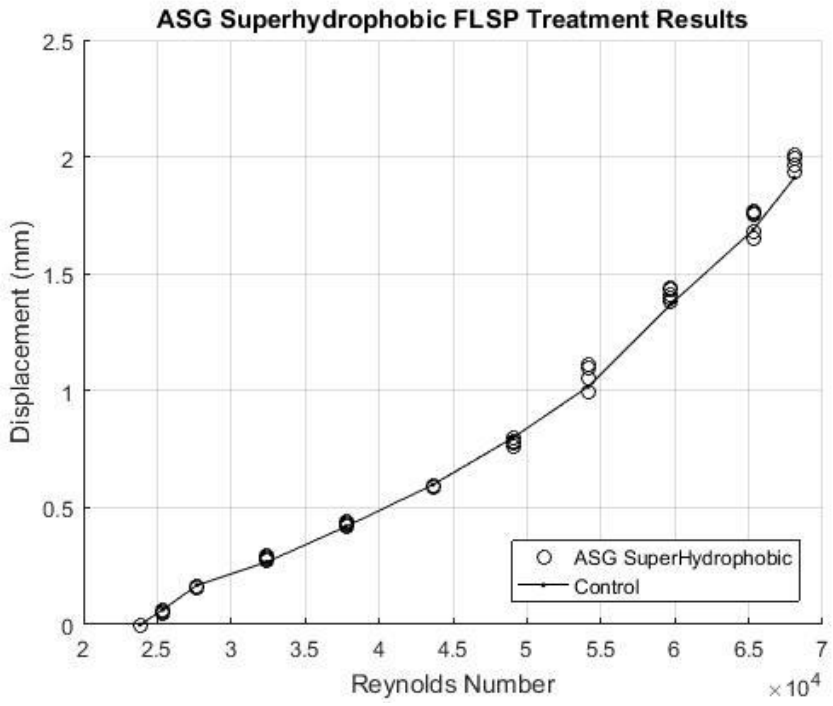

Figure 15. Displacement results from ASG superhydrophobic tests

The ASG superhydrophobic results show overall less displacement than the BSG superhydrophobic plate, but still more drag on average than the untreated control plate. It would appear that the Cassie state is transitioning to a Wenzel state while the plate is submerged, but the resultant roughness is having a smaller effect than BSG treatment.

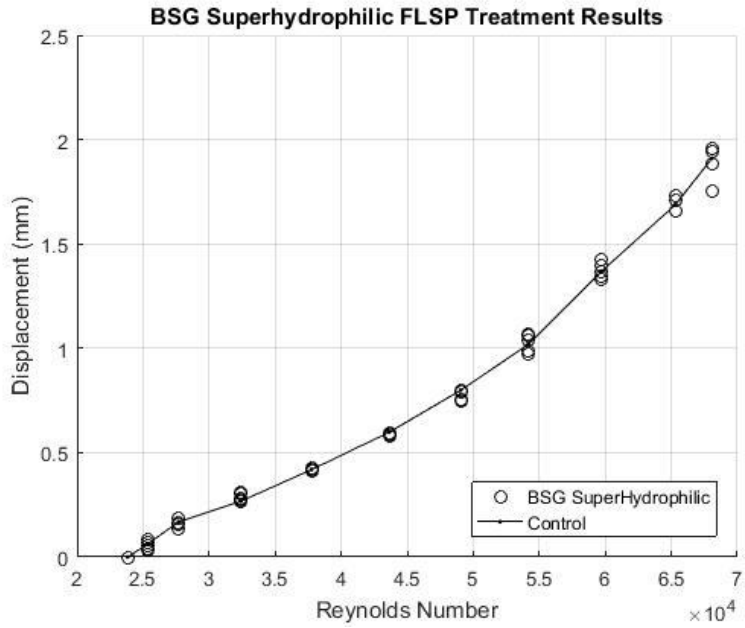

Figure 16. Displacement results from BSG superhydrophilic tests

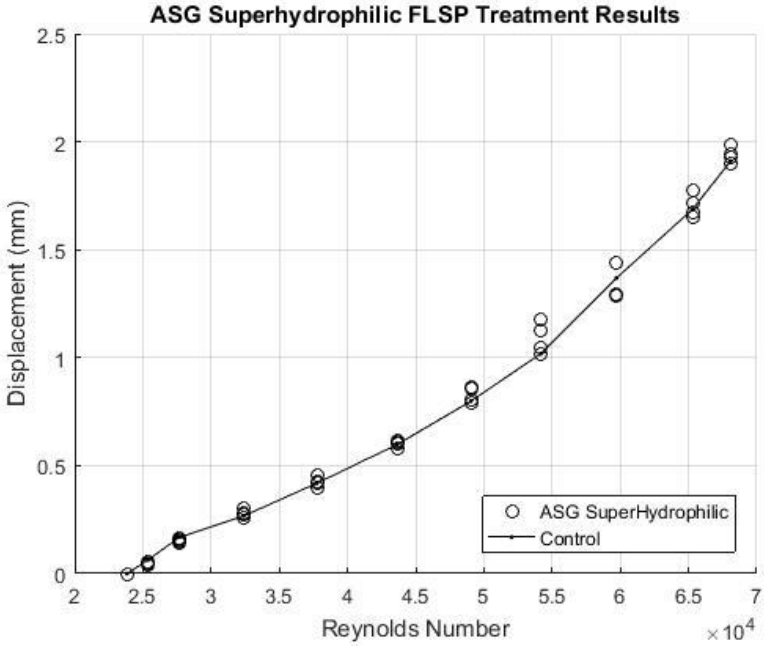

Figure 17. Displacement results from ASG superhydrophilic tests

Each of the superhydrophilic FLSP treatments performed as expected in the displacement tests. The wicking action of the plate enforces a zero slip condition that serves to create similar friction characteristics to the untreated control plate across all flow conditions. There was no unique performance indication by either the BSG nor ASG superhydrophilic samples. Both of the superhydrophilic samples retained their properties throughout the duration of submerged testing and storage for over 6 months.

Total force was derived from the average displacement for each plate with the intent of determining the effect of skin friction in each test. Since both plates show an increase in skin drag force due to friction over the control plate, Figure 18 is the difference between the BSG and ASG total forces that shows how each surface geometry contributes to roughness indicated in the tests.

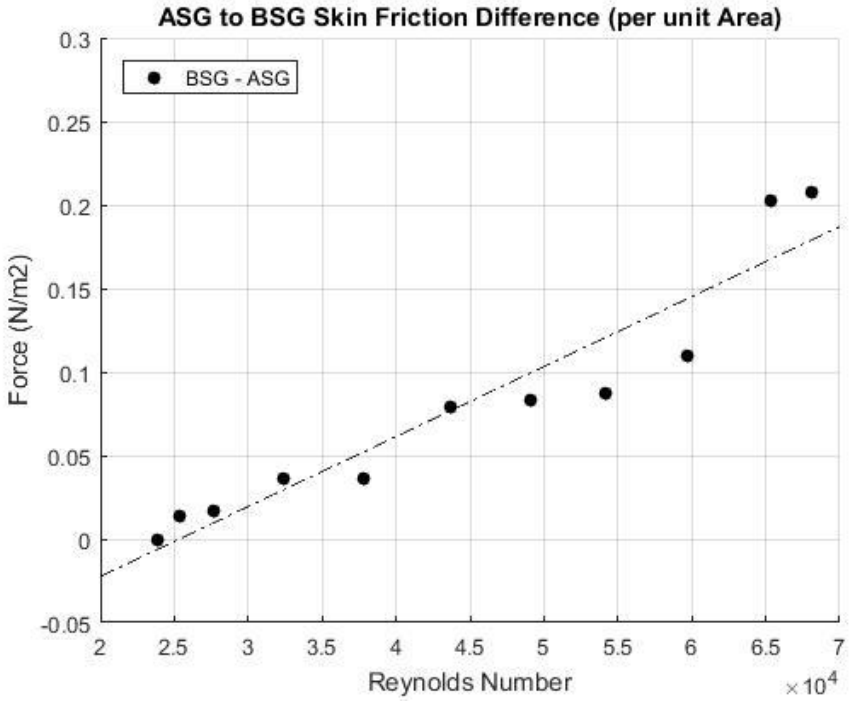

Figure 18. Difference in force due to skin friction between BSG and ASG

The ASG superhydrophobic plate appears to have better skin friction performance than the BSG plate, but neither better in a fully submerged flow field than the control plate.

The next section will discuss the source of this phenomenon in a study of the Cassie state stability of each of the superhydrophobic surface structures.

B. CASSIE STATE STABILITY

The displacement results indicated that the water flowing over the surface of the superhydrophobic surfaces was seeing roughness instead of slipping along an air layer as expected with the existence of a Cassie state. Upon closer observation, a gradual breakdown of the Cassie state was observed to occur on the surfaces of both the BSG and ASG superhydrophobic test plates while submerged in water over a short period of time without any flow over the surface. Figure 19 shows the surface of the BSG superhydrophobic plate immediately after wetting at low magnification. Raising the magnification yields Figure 20, which shows how the individual air pockets have formed over the surface of the BSG formations. The bright areas on the plate are air pockets, and the darker area represents interfaces between high points on the layer.

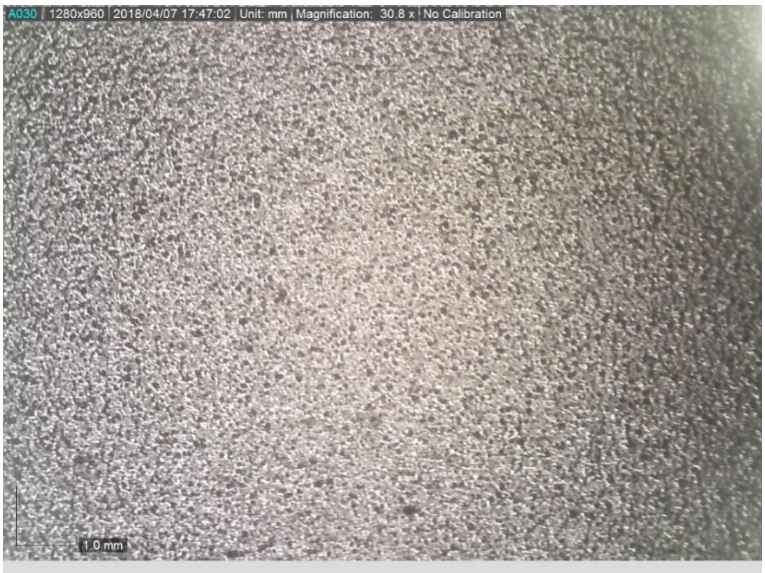

Figure 19. BSG superhydrophobic after initial wetting (30x)

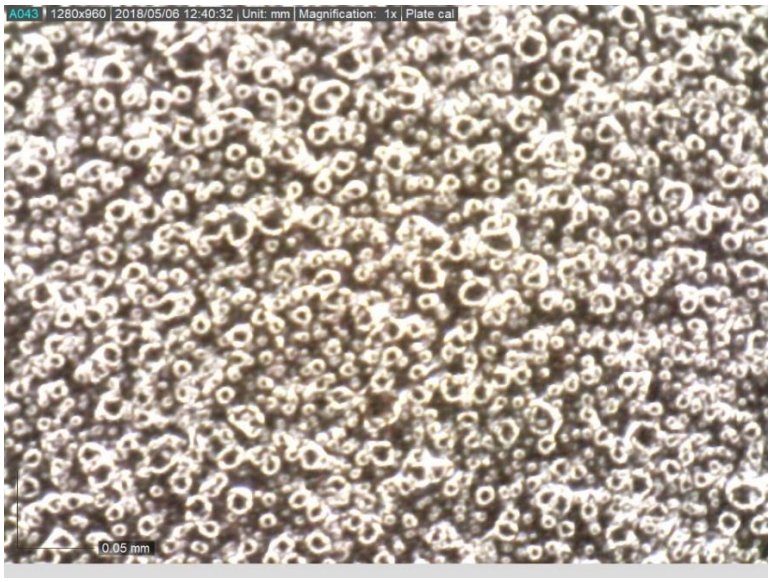

Figure 20. BSG superhydrophobic after initial wetting (140x)

The air layer on the surface of the BSG plate was observed for approximately 15 minutes until it appeared that much of the Cassie state on the surface had transitioned to a partial Wenzel state. The resulting appearance on the surface after the transition is presented in Figure 21.

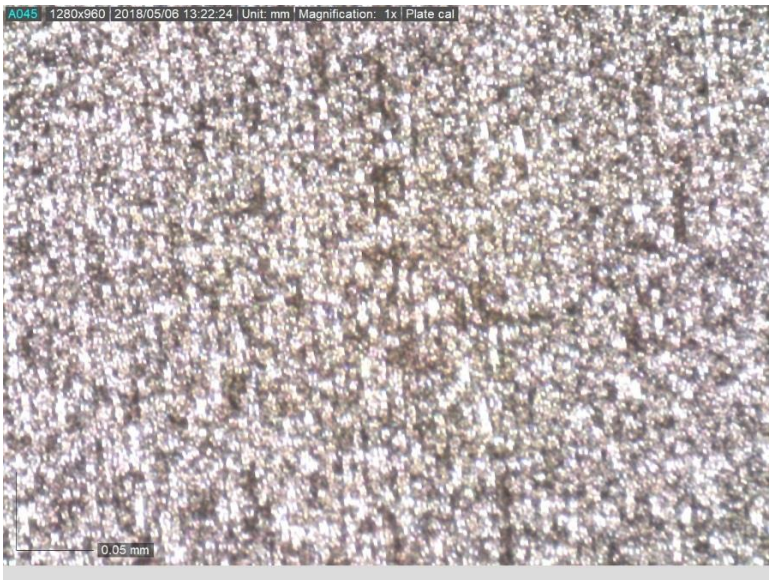

Figure 21. BSG superhydrophobic after extended submergence (140x)

It is clear to see by the geometric uniformity of the FLSP treated surface that the peaks are protruding beyond the air layer. The air appears to have been pushed into the valleys between the BSG mounds while under static pressure from the water. This effect is better observed on the ASG superhydrophobic plate, whose surface is shown after initial wetting in Figures 22 and 23.

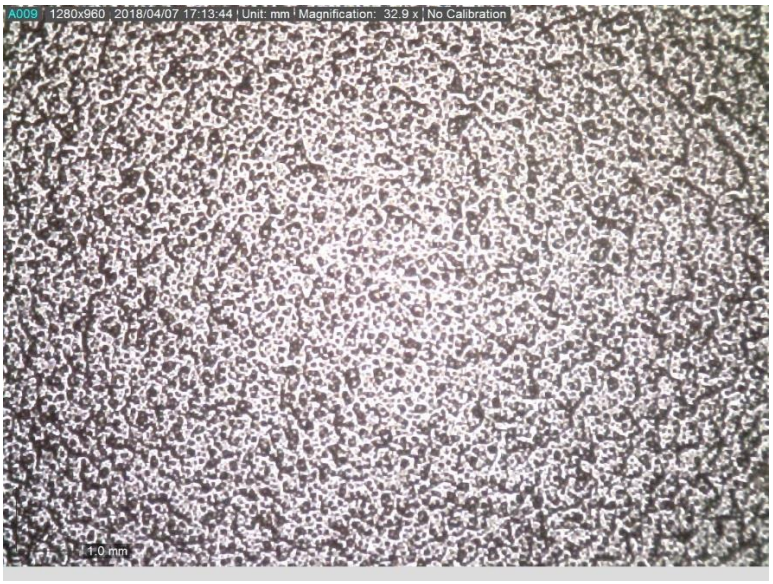

Figure 22. ASG superhydrophobic after initial wetting (33x)

Figure 23. ASG superhydrophobic after initial wetting (140x)

The ASG superhydrophobic surface has larger features in the air layer that are suspended above the structure after wetting. The elongated bright areas indicate curvature in the air-water interface where high points interface with planar portions of the air layer. The air layer on the ASG superhydrophobic surface appeared to transition more slowly to the Wenzel state than did the BSG superhydrophobic surface. Notable was the increasing density of the circular features in the images over time. Approximately 40 minutes after being submerged, the uniform transition to a partial Wenzel state on the ASG superhydrophobic surface displayed the features in Figure 24.

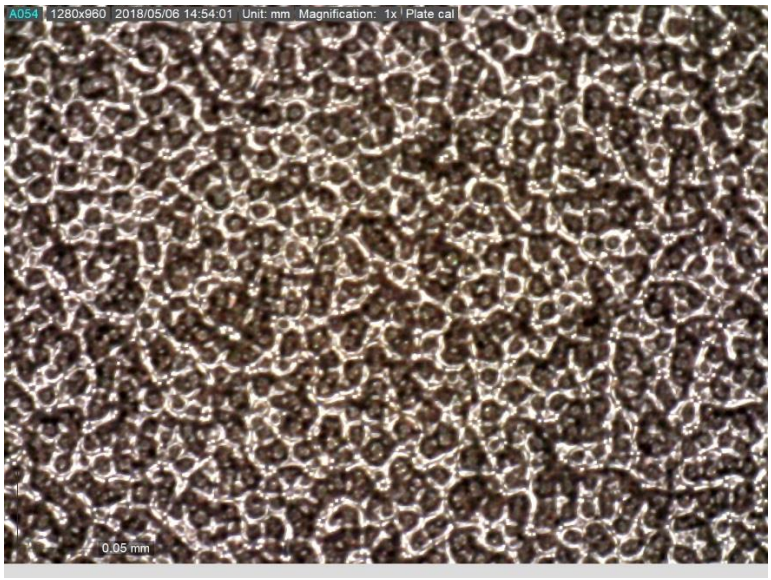

Figure 24. ASG superhydrophobic after extended submergence (140x)

The channels of air pockets trapped between the peaks are clearly visible as the bright lines between the darker peaks of the surface structure. This image serves to confirm that there are peaks on both the BSG and ASG superhydrophobic surfaces exposed to the water after a short duration fully submerged. Raising the water pressure by filling the channel further accelerated the transition for both surface types. In all cases, superhydrophobic properties were recovered as soon as the plate was removed from the water.

C. BIOFOULING

The biofouling results are linked to a combination of the breakdown of the Cassie state as well as the susceptibility of salt corrosion observed by James Ley [33]. The FLSP treated test plates retain moisture in a condensate environment that promotes anodic corrosion as well as a strong environment for marine biological growth.

Microbial buildup in a film layer was immediately observable on the top and bottom of both plates after 14 days. The top of each of the samples are shown in Figures 25 and 26 for the control plate and BSG superhydrophobic plate respectively. The bottoms of each plate differed only in the sediment buildup. Microbial film was present throughout as well as rust along the edges of the plates.

Figure 25. 14 day biological growth on control

Figure 26. 14 day biological growth on BSG

The test was continued in order to observe macrofouling at a visually evident level. Both plates were affected by macrofouling at the same relative degree as indicated by the plant and animal life on the top and bottom of both plates. The experiment results followed the predicted timeline for the presence of larvae and other forms of growth [36]. Based on the appearance of the samples in Figures 27 and 28, it is evident that the FLSP treatment has no intrinsic defense against biofouling.

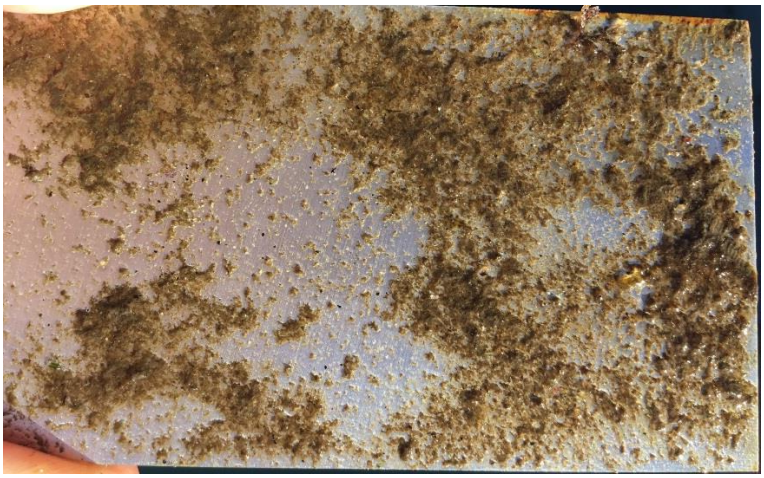

Figure 27. 24 day biological growth on control

Figure 28. 24 day biological growth on BSG

IV. CONCLUSIONS AND RECOMMENDATIONS

A. CONCLUSIONS

Superhydrophobic and superhydrophilic properties applied through femtosecond surface laser processing to industrial and metallic materials have a vast range of potential applications. The objective of these experiments were to analyze the behavior of FLSP surfaces in a fully submerged environment for skin drag performance, Cassie state stability, and resiliency against biological fouling.

Displacement testing was conducted in a custom designed flow channel capable of sensing displacement caused by fluid flow across the surfaces of two sample plates. The tests were repeated several times per sample for flow rates ranging from 227.12 – 832.79 L/min (60 – 220 gpm). Untreated control plates were tested to determine a baseline displacement curves. Sample plates consisting of FLSP treated surfaces exhibiting superhydrophobic and superhydrophilic properties were tested against the control performance. Both the BSG and ASG superhydrophobic samples showed larger displacements than the control that increased consistently with Reynolds number. The BSG superhydrophobic sample showed a larger relative skin friction to the control than did the ASG superhydrophobic sample. The samples did not perform consistently with superhydrophobic surface theory because of a loss of superhydrophobic properties that occurred following complete submergence in water.

A portable microscope was used to analyze the stability of the Cassie state on each of the FLSP superhydrophobic samples. The samples were submerged in water for an extended period of time and observed from above. The presence of an air layer over the surface of each sample after initial wetting confirmed the presence of the Cassie state and, as such, superhydrophobic properties. However, the duration of the Cassie state was limited on both plates, and the Cassie state observed to transition to a partial Wenzel state and lose superhydrophobic properties after 15 minutes for the BSG superhydrophobic sample and 40 minutes for the ASG superhydrophobic sample. These results served to explain the unexpectedly high skin drag results in the displacement tests.

Finally, an experiment was performed to determine the resiliency of FLSP superhydrophobic surfaces against biological growth and fouling in a marine environment. Two samples, an untreated control plate, and a BSG superhydrophobic plate were suspended in tubes below a floating dock at an active pier in Monterey Bay for 24 days. The results of the biofouling test was consistent with previous findings that FLSP superhydrophobic surfaces lack long term resistance to salt corrosion, and found those results to be a factor in biological growth. Strong evidence of microbiological activity was present after 14 days. Plant and animal life were both present on the surfaces of each sample before the experiment was finished on the 24th day.

These experiments found that a functionalized superhydrophobic surface created by femtosecond laser surface processing is unstable in a fully submerged marine environment in the configurations that were tested. However, the functionalized superhydrophilic surfaces performed exactly as designed and showed no signs of degradation after 6 months in both wet and dry environments.

B. RECOMMENDATIONS

It is recommended that further study of the Cassie state stability of FLSP treated superhydrophobic surfaces be conducted to examine the operating envelope of these materials. Enhanced understanding of the formation and transformation of the Cassie state on a functionalized superhydrophobic surface can be realized through additional microscopic observation under tightly controlled submerged conditions. Specific water pressures and associated transition times should be studied to find any unique parameters associated with the Cassie state on each BSG and ASG superhydrophobic surfaces.

The displacement testing has value in determining the skin friction of these and future material studies. The shape and size of the sample plates should be redesigned to enhance the perceptibility of the effect of skin friction and minimize errors caused by flow oscillations over the blunt leading edge. The stability of the samples in high Reynolds number flows would be enhanced with a more robust mounting arrangement.

APPENDIX. SENSOR CALIBRATIONS

Displacement Sensor Calibration Report
LORD MicroStrain®
Date: 8/3/2017

Sensor Model: 6101-0100
Sensor Serial Number: 67126

Signal Conditioner Model: 6130-1110
Signal Conditioner Serial Number: 67242

Polynomial Fit

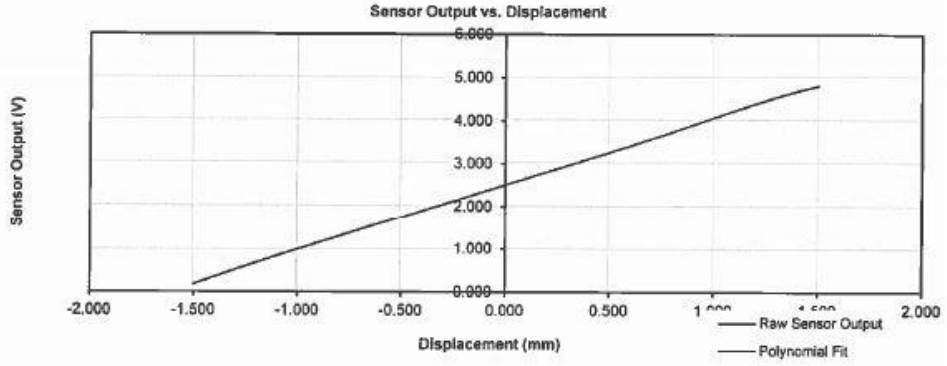

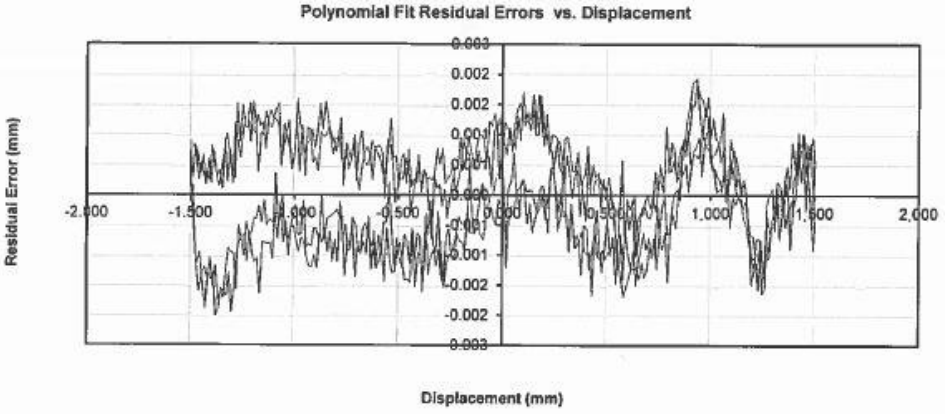

Polynomial Fit Model

$D = A0 + A1*x + A2*x^2 + A3*x^3 + \ldots$

where D = Displacement (mm)
Ai = ith order Polynomial Coefficient
x = Sensor Output (V)

Polynomial Fit Results

Coefficient	Value
A0	-1.59462E+00
A1	5.56979E-01
A2	5.04251E-02
A3	2.62717E-02
A4	-4.08484E-02
A5	1.84327E-02
A6	-3.67071E-03
A7	2.71721E-04

Displacement Sensor Calibration Report
LORD MicroStrain®

Date: 8/3/2017

Sensor Model: 6101-0100
Sensor Serial Number: 67127

Signal Conditioner Model: 6130-1110
Signal Conditioner Serial Number: 67243

Polynomial Fit

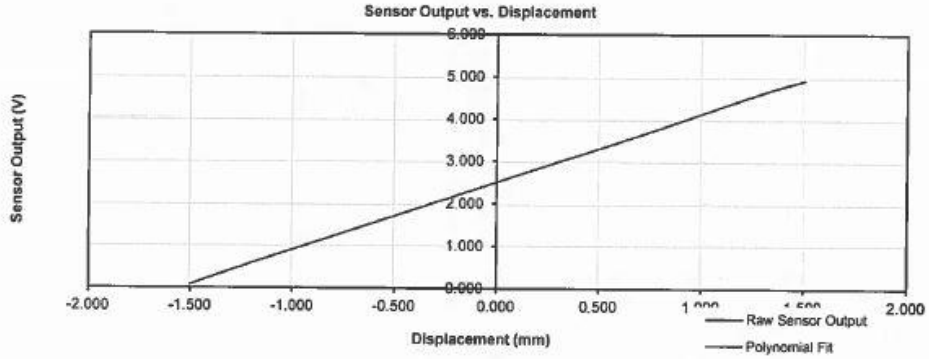

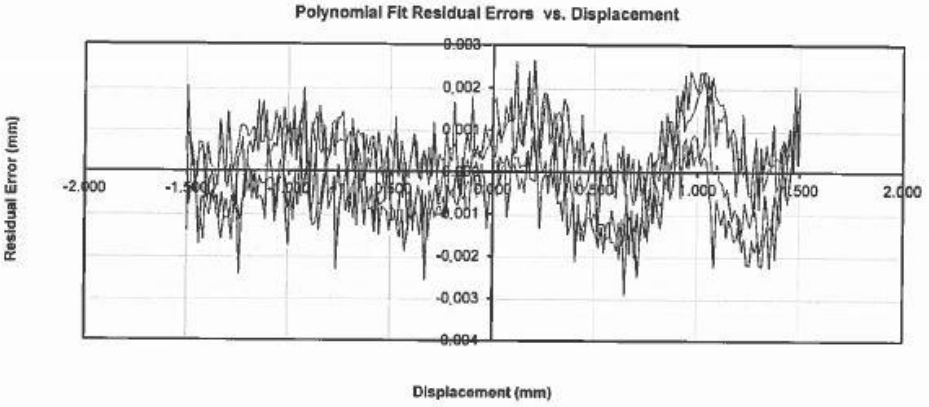

Polynomial Fit Model

$D = A0 + A1*x + A2*x^2 + A3*x^3 + ...$

where D = Displacement (mm)
Ai = ith order Polynomial Coefficient
x = Sensor Output (V)

Polynomial Fit Results

Coefficient	Value
A0	-1.54122E+00
A1	5.65424E-01
A2	2.69639E-02
A3	3.52730E-02
A4	-4.34017E-02
A5	1.85241E-02
A6	-3.52271E-03
A7	2.49510E-04

LIST OF REFERENCES

[1] G. Batchelor, *An Introduction to Fluid Dynamics*. Cambridge, UK: Cambridge Univ. Press, 2000.

[2] T. Min and J. Kim, "Effects of hydrophobic surface on skin-friction drag," *Physics of Fluids*, vol. 16, no. 7, 2004.

[3] C. L. M. H. Navier, "Mémoire sur les lois du mouvement des *fluids* (Memory on the Laws of Fluid Motion)," *Paris, France; Mémoires de l'Académie Royale des Sciences de l'Institut de France*, pp. 389–440, 1823.

[4] A. Cassie and S. Baxter, "Wettability of porous surfaces," *Transactions of the Faraday Societ*y, vol. 40, pp. 546, 1944.

[5] C. Neinhuis and W. Barthlott, "Characterization and distribution of water-repellent, self-cleaning plant surfaces," *Annals of Botany*, vol. 79, no. 6, pp. 667–677, 1997.

[6] B. Bhushan, and P. L. Ko, "Introduction to Tribology," *Applied Mechanics Reviews*, vol. 56, no. 1, 2003.

[7] B. Bhushan, and Y. Jung, "Micro- and nanoscale characterization of hydrophobic and hydrophilic leaf surfaces," *Nanotechnology*, vol. 17, no. 11, pp. 2758–2772, 2006.

[8] R. N. Wenzel, "Resistance of solid surfaces to wetting by water," *Ind. Eng. Chem.*, vol. 28, pp. 988–994, 1936.

[9] S. Lyu, D. C. Nguyen, D. Kim, W. Hwang, and B. Yoon, "Experimental drag reduction study of super-hydrophobic surface with dual-scale structures," *Applied Surface Science*, vol. 286, pp. 206–211, 2013.

[10] B. Bhushan, "Nanotribology and nanomechanics," *Wear*, vol. 259, no. 7, pp. 1507–1531, 2005.

[11] J. Long, L. Pan, F. Lin, G. Peixun, J. Dingwei, D. Jiang, H. Zhang, L. Li, and M. Zhong, "Cassie-state stability of metallic superhydrophobic surfaces with various micro/nanostructures produced by a femtosecond laser," *Langmuir : the ACS journal of surfaces and colloids*, vol. 32, no. 4, pp. 1065, 2016.

[12] H. Gu, C. Wang, S. Gong, Y. Mei, H. Li, W. Ma, "Investigation on contact angle measurement methods and wettability transition of porous surfaces," *Surface & Coatings Technology*, vol. 292, pp. 72–77, 2016.

[13] J. Rothstein, "Slip on superhydrophobic surfaces," *Annu. Rev. Fluid Mech.*, vol. 42, no. 1, pp. 89–109, 2010.

[14] A. Lafuma, and D. Quéré, "Superhydrophobic states," *Nature Materials*, vol. 2, no. 7, pp. 457, 2003. (July 2003): 457.

[15] J. Ou, G. Moss, J. Rothstein, "Enhanced mixing in laminar flows using ultrahydrophobic surfaces," *Physical review. E, Statistical, Nonlinear, and Soft Matter Physics*, vol. 76, no. 1 Pt 2, 2007.

[16] Y. Takata, S. Hidaka, J.M. Cao, T. Nakamura, H. Yamamoto, M. Masuda, and T. Ito, "Effect of surface wettability on boiling and evaporation," *Energy*, vol. 30, no. 2, pp. 209–220, 2005.

[17] H. Hsu, M. Lin, B. Popovic, C. Lin, N. Patankar, and Y. Mishra, "A numerical investigation of the effect of surface wettability on the boiling curve," *PLoS ONE* vol. 12, no. 11, 2017.

[18] P. Raturi, K. Yadav, and J. Singh, "ZnO-Nanowires-Coated Smart Surface Mesh with Reversible Wettability for Efficient On-Demand Oil/Water Separation," *ACS Applied Materials & Interfaces*, vol. 9, no. 7, pp. 6007–6013, 2017.

[19] L. Feng, Y. Song, J. Zhai, B. Liu, J. Xu, L. Jiang, D. Zhu, "Creation of a Superhydrophobic Surface from an Amphiphilic Polymer," *Angewandte Chemie International Edition*, vol. 42, pp. 800–802, 2003.

[20] J. Kim and C.J. Kim, "Nanostructured surfaces for dramatic reduction of flow resistance in droplet-based microfluidics," *Technical Digest. MEMS 2002 IEEE International Conference. Fifteenth IEEE International Conference on Micro Electro Mechanical Systems (Cat. No.02CH37266)*, Las Vegas, NV, USA, pp. 479–482, 2002.

[21] K. Tadanga, J. Morinaga, A. Matsuda, and T. Minami, "Superhydrophobic-superhydrophilic micropatterning on flowerlike alumina coating film by the sol-gel method," *Chem. Mater.*, vol. 12, pp. 590–592, 2000.

[22] J. Youngblood and T. McCarthy, "Ultrahydrophobic polymer surfaces prepared by simultaneous ablation of polypropylene and sputtering of poly(tetraflouroethylene) using radio frequency plasma," *Macromolecules*, vol. 32, pp. 6800–6806, 1999.

[23] H. Liu, L. Feng, J. Zhai, L. Jiang, and D. Zhu, "Reversible wettability of a chemical vapor deposition prepared zno film between superhydrophobicity and superhydrophilicity," *Langmuir*, vol. 20, no. 14, pp. 5659–5661, 2004.

[24] D. Kim, W. Hwang, H. Park, and K. Lee, "Superhydrophobic nano-wire entanglement structures," *J. Micromech. Microeng.*, vol. 16, pp. 2593–2597, 2006.

[25] S. Sethi and A. Dhinojwala, “Superhydrophobic conductive carbon nanotube coatings for steel,” *Langmuir*, vol. 25, no. 8, pp. 4311–4313, 2009.

[26] M. Barberoglou, V. Zorba, E. Stratakis, E. Spanakis, P. Tzanetakis, S.H. Anastasiadis, and C. Fotakis, “Bio-inspired water repellent surfaces produced by ultrafast laser structuring of silicon,” *Applied Surface Science* vol. 255, no. 10, pp. 5425–5429, 2009.

[27] T.O. Yoon, H.J. Shin, S.C. Jeoung, and Y. Park, “Formation of superhydrophobic poly(dimethysiloxane) by ultrafast laser-induced surface modification,” *Optics Express* vol. 16, no. 17, p. 12715, 2008.

[28] A. Kietzig, S. Hatzikiriakos and P. Englezos, “Patterned superhydrophobic metallic surfaces,” *Langmuir*, vol. 25, no. 8, pp. 4821–4827, 2009.

[29] C. Zuhlke, T. Anderson, D. Alexander, “Comparison of the structural and chemical composition of two unique micro/nanostructures produced by femtosecond laser interactions on nickel,” *Appl. Phys. Lett.*, vol. 103, no. 121603, 2013.

[30] C. Zuhlke, T. Anderson, P. Li, M. Lucis, N. Roth, J. Shield, B. Terry and D. Alexander, “Superhydrophobic metallic surfaces functionalized via femtosecond laser surface processing for long term air film retention when submerged in liquid,” *Laser-based Micro- and Nanoprocessing IX*, 2015.

[31] G. Romer, A.J. Huis, J. Meijer, and M.N.W. Groenendijk, “On the formation of laser induced self-organizing nanostructures,” *CIRP Annals – Manufacturing Technology*, vol. 58, no. 1, pp. 201–204, 2009.

[32] E. Peng, A. Tsubaki, C. Zuhlke, M. Wang, R. Bell, M. Lucis, T. Anderson, D. Alexander, G. Gogos, and J. Shield, “Micro/nanostructures formation by femtosecond laser surface processing on amorphous and polycrystalline Ni60Nb40,” *Applied Surface Science*, vol. 396, pp. 1170–1176, 2017.

[33] J. Ley, “Hydrodynamic drag force measurement of a functionalized surface exhibiting superhydrophobic properties,” Master’s thesis, Naval Postgraduate School, 2016.

[34] Microminiature Gauging DVRT® | LORD Sensing Systems (2017) Microstrain.com. [Online]. Available: http://www.microstrain.com/displacement/mg-dvrt

[35] Edge Series Microscopes | DinoLite (2018) Dinolite.us. [Online]. Available: www.dinolite.us/products/digital-microscopes/usb/edge-series-all/am73915mztl

[36] D. Yebra, S. Kiil, K. Dam-Johansen, “Antifouling technology – past, present and future steps towards efficient and environmentally friendly antifouling coatings,” *Progress in Organic Coatings* vol. 50, pp. 75–104, 2004.

THIS PAGE INTENTIONALLY LEFT BLANK

INITIAL DISTRIBUTION LIST

1. Defense Technical Information Center
   Ft. Belvoir, Virginia

2. Dudley Knox Library
   Naval Postgraduate School
   Monterey, California